PERGAMON

Journal of Structural Geology 21 (1999) 635–652

JOURNAL OF STRUCTURAL GEOLOGY

# Lateral propagation of the surface trace of the South Alkyonides normal fault segment, central Greece: its impact on models of fault growth and displacement–length relationships

Nigel C. Morewood*, Gerald P. Roberts

*The Research School of Geological and Geophysical Sciences, Birkbeck and University College London, Gower Street, London WC1E 6BT, UK*

Received 17 July 1998; accepted 10 February 1999

**Abstract**

The evolution of deformed marine terraces and drainage systems have been examined in order to investigate the growth and lateral propagation of an active normal fault. Geological mapping has revealed three distinct raised marine terraces in the immediate footwall of the western end of the active South Alkyonides Fault Segment (SAFS), Gulf of Corinth, central Greece. We correlate these terraces with sea-level highstands at 125, 240 and 330 ka. Using elevation estimates of the inner edges of the terraces we show that uplift rates decrease towards the Perachora Fault Segment Boundary at the western end of the SAFS. Analysis of terraces and drainage wind gaps in the footwall of the fault shows that the surface trace of the SAFS propagated westwards at a rate of 12.1–16.7 mm/y over at least the last 330 ka. Whilst the surface trace length has increased, analysis of the geometry and kinematics of fault-slip suggests that fault length at depth has remained fixed, implying progressive increase in the values for the displacement–length ratio. If this is correct, growth is not self-similar and fault length has been established early in the evolution of the system, i.e. before 330 ka. © 1999 Elsevier Science Ltd. All rights reserved.

## 1. Introduction

Lateral propagation is commonly mentioned when discussing fault growth. It is generally agreed that as a fault accumulates displacement, the fault surface must grow in size because the fault length ($L$) scales with displacement ($d$) in the form of $d = \gamma L$ (e.g. Walsh and Watterson, 1988; Cowie and Scholz, 1992a) (Fig. 1a). However, data concerning the growth of normal faults from field observations are rare. Jackson and Leeder (1994) studied how the propagation of the Pearce Scarp, Pleasant Valley (USA) affected drainage development and estimated a rate at which lateral propagation was occurring. Jackson et al. (1996) used drainage patterns to demonstrate fold and fault growth associated with active reverse faults in New Zealand. Gawthorpe et al. (1997) inferred how strata are affected in the immediate vicinity of a propagating normal fault tip and how stratigraphy might change along the strike of active normal fault systems.

The lack of field observations is worrying because the details of propagation underpin several aspects of existing fault growth models. For example, (1) if a fault propagates along strike in the manner shown in Fig. 1(a) then it increases the surface area of the fault plane. Thus, the seismic moment associated with that fault must increase with time, even if the displacement rate remains constant, because the moment is a function of fault plane area (Nicol et al., 1997). These authors concluded that constant regional strain rate can be accommodated by establishing fault lengths at an early stage (e.g. Fig. 1b) and slowing lateral propagation by fault interaction, or by decreasing the number of active faults with time. Clearly, it is important to understand the relationship between fault propagation and fault plane surface area if we are to decide how many active faults are needed—within a given volume—to accommodate the regional strain rate. (2)

* Corresponding author.
*E-mail address:* n.morewood@ucl.ac.uk (N.C. Morewood)

0191-8141/99/$ - see front matter © 1999 Elsevier Science Ltd. All rights reserved.
PII: S0191-8141(99)00049-8

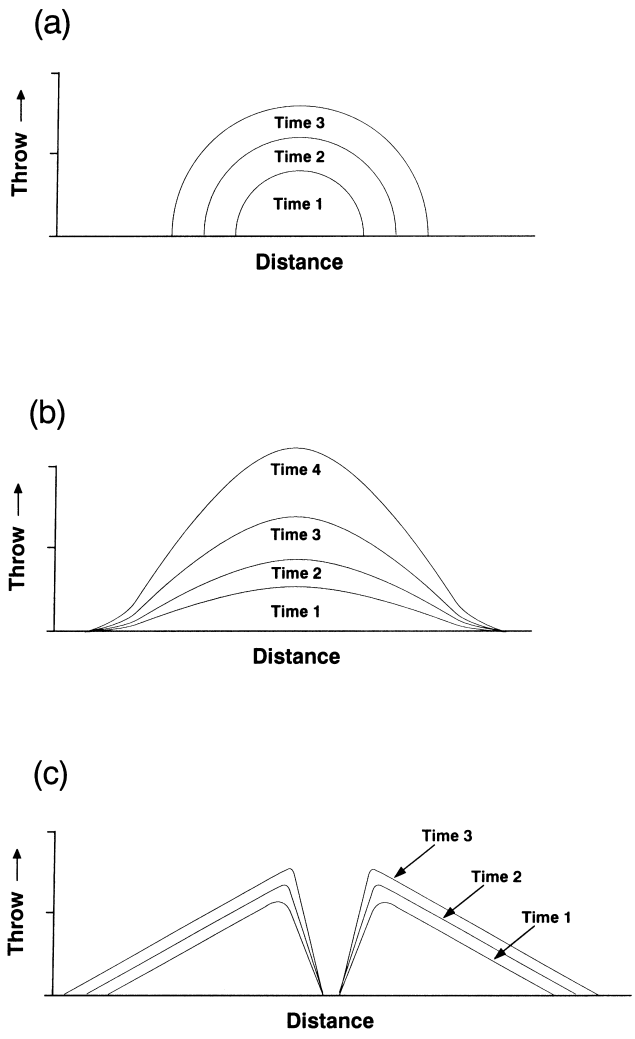


Fig. 1. Schematic throw–distance profiles for (a) a fault which is laterally propagating at depth, (b) a fault with its ends fixed at depth and (c) two faults lying along-strike of one another. The faults in (c) show restricted growth and increased throw gradients towards their shared segment boundary (after Nicol et al., 1996).

Faults that lie along strike from each other and are mechanically interacting may develop increased displacement gradients at their shared segment boundary (Fig. 1c; Nicol et al., 1996). Fig. 1(b) shows that one way to develop this is for the fault length to be fixed at depth, at least over the time period when the faults are interacting. In this paper we describe field observations which we use to test various characteristics of the growth models described above.

Our approach is unusual because, although workers have used marine terraces to describe growth of structures in two dimensions—generally along transects perpendicular to strike—we are unaware of studies using marine terraces to investigate fault propagation along strike. The terraces we use are ideal for this because they are exposed along the strike and close to the tip of an active normal fault. In this paper we use geological and geomorphological observations to show that the surface trace of the western end of the South Alkyonides Fault Segment (SAFS) has propagated westwards over at least the past c. 330 ka. We have mapped raised marine deposits on the southern side of the Perachora Peninsula, which lie in the immediate footwall of the SAFS, and distinguish three distinct terraces which we correlate with the sea-level high-stands at 330, 240 and 125 ka (Figs. 2–4). Using the uplift rates derived from the elevations of the inner edges of these marine terraces we estimate rates of uplift within the footwall of the western end of the SAFS and show how these vary as the Perachora Fault Segment Boundary (PFSB) is approached. We also present data to show that individual drainage channels have been systematically beheaded as the fault tip has propagated. The marine terraces allow us to date truncation of these channels. We use this information to propose a growth model for the SAFS, including a rate of tip propagation, and to show how the Perachora Peninsula has evolved both geologically and geomorphologically over the past 330 ka.

## 2. Geological and tectonic setting of the Perachora Peninsula

The Perachora Peninsula lies at the eastern end of the Gulf of Corinth, central Greece, one of the fastest extending regions of the Earth's continental crust [c. 10 mm/y of N–S extension (Billiris et al., 1991)]. Extension across the Gulf of Corinth is accommodated by a system of segmented normal faults (Roberts and Jackson, 1991; Armijo et al., 1996; Roberts, 1996a,b). The western part of the Perachora Peninsula forms a complexly deformed segment boundary between the ends of two c. E–W-striking normal faults, the Xilokastro Fault Segment (XFS) to the west and the SAFS to the east (Morewood and Roberts, 1997) (Figs. 2 and 3). The Neogene–Recent stratigraphy of the Perachora Peninsula comprises uplifted beach–shoreface deposits of Pleistocene age overlying deeper water Pliocene marls (IGME, 1984).

Fault-slip data show a systematic variation in slip direction along the SAFS with nearly pure dip-slip at the centre and a large component of along-strike motion and extension at the ends (Roberts, 1996a,b; Morewood and Roberts, 1997) (Figs. 2 and 3). The maximum cumulative throw is c. 2.5–3.0 km and occurs in the central portion of the SAFS between Skinos and Alepochori (Myrianthis, 1982; Perissoratis et al., 1986; Roberts, 1996b). The throw decreases from c. 1360 m, near Skinos, to c. 20 m, at Lake Vouliagmeni, over a distance of 15 km (Figs. 3a, 4 and 5). Near the villages of Pisia and Perachora, the throw

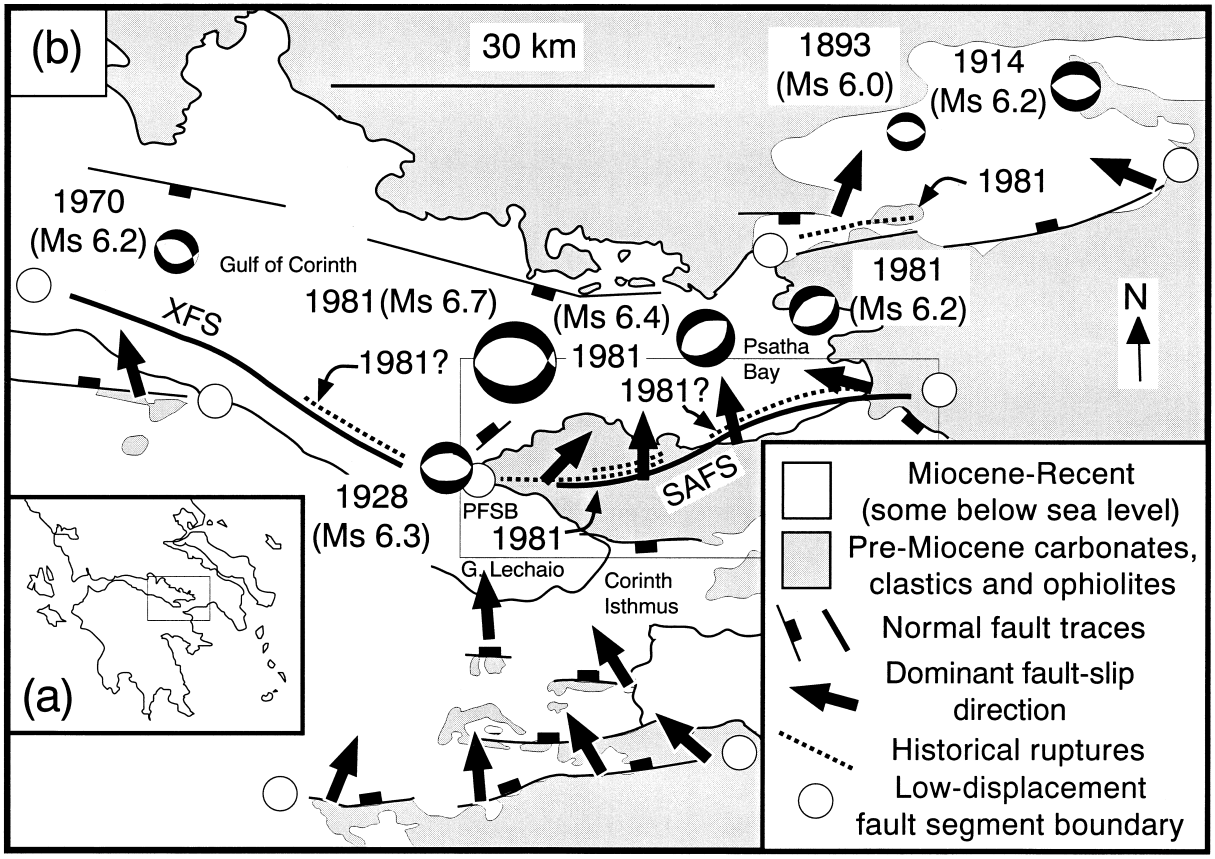


Fig. 2. (a) Map of Greece. Inset box locates (b). (b) Map showing the segmented normal fault system at the eastern end of the Gulf of Corinth. Thick lines identify the Xilokastro (XFS) and South Alkyonides (SAFS) Fault Segments. PFSB indicates the Perachora Fault Segment Boundary. Focal mechanisms are shown for all earthquakes > Ms 6.0 since 1893 (from Billiris et al., 1991). Known and suspected surface ruptures are from Jackson et al. (1982), Abercrombie et al. (1995) and Hubert et al. (1996). Dominant fault-slip directions are from Roberts (1996a). Inset box locates Fig. 3.

is c. 450 m (Fig. 3a). The throw is also observed to decrease towards the eastern end of the SAFS (Roberts and Gawthorpe, 1995; Roberts, 1996b). The western end of the SAFS was ruptured at the surface during the 1981 Alkyonides earthquake sequence (Ms 6.7, Ms 6.4) and coseismic throws were observed to decrease towards the PFSB (Jackson et al., 1982). The eastern end of the XFS may have been ruptured in 1928 (Ms 6.3) and 1981 (Ambraseys and Jackson, 1990; Abercrombie et al., 1995; Hubert et al., 1996).

In contrast to the simple converging pattern of slip along the SAFS, the structure and kinematics within the PFSB is complex (Morewood and Roberts, 1997) (Fig. 3b). Within this fault segment boundary, contemporaneous c. N–S and c. E–W dip- and oblique-slip faulting has occurred over at least the past 125 ka and the summed rates of E–W and N–S extension are similar. The deformation within the PFSB is oblate vertical flattening (Morewood and Roberts, 1997).

## 3. Deformed marine terraces

### 3.1. Introduction and previous work

Marine terraces that step upwards and landward from active shorelines are thought to be the product of interplay between the rate of global sea-level change and the rate of tectonic uplift (e.g. Chappell, 1974; Lajoie, 1986; Valensise and Ward, 1991). Such terraces have a natural upward slope landwards and are generally erosional. They are often covered by colluvium from palaeo-sea-cliffs and by down-washed deposits from further upslope or shoreface marine sediments. Thus, the only horizontal reference to sea-level on an

uplifted marine terrace is the mapped trace of palaeo-shoreline positions at the most landward extent of the terrace. These inner edges naturally form at the base of palaeo-sea-cliffs and their elevations are precise markers of the amount of uplift from the sea-level at which they formed.

Glacio-eustatic sea-level changes occur much more rapidly than long-term coastal uplift (Chappell and Shackleton, 1986). Thus, stepped marine terraces can act as a record of Pleistocene sea-level highstands over-printed on the longer-term tectonic coastal uplift (Armijo et al., 1996). Terraces formed during sea-level lowstands are usually eroded by wave action and subsequently covered by highstand sediments (Lajoie, 1986). The ages of sea-levels at highstands are well-constrained over the past 330 ka (Chappell and Shackleton, 1986; Merritts and Bull, 1989), so highstand terraces on uplifting coastlines are commonly preserved and available for examination and use as strain markers.

Pleistocene marine terraces have been described on the Perachora Peninsula and elsewhere around the

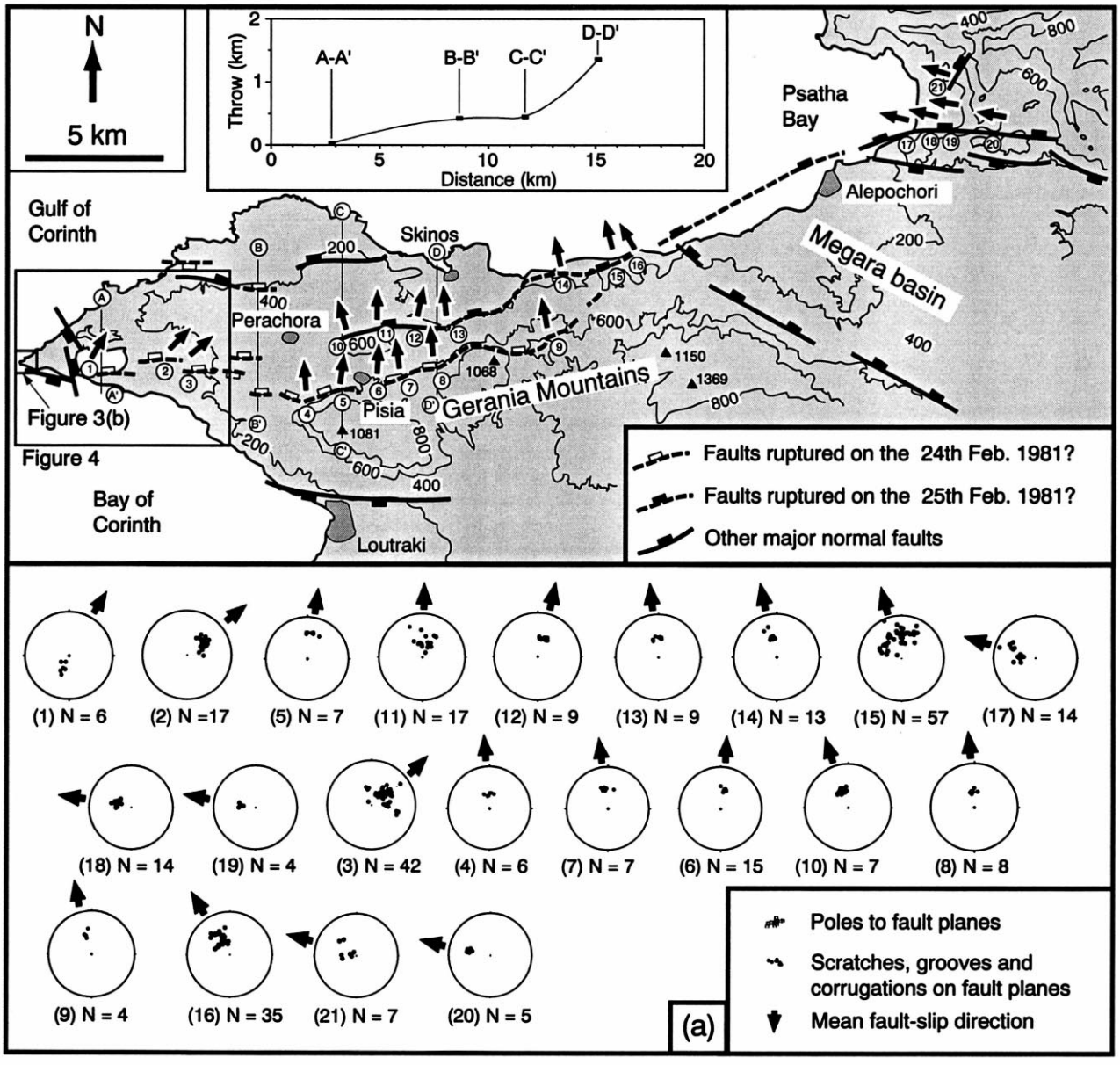


Fig. 3.. (a) Map and stereographic projections showing the systematic variation in slip direction along the South Alkyonides Fault Segment (SAFS). Note the oblique-slip towards the hanging wall at the ends of the fault and the dip-slip at the centre. The upper box shows how throw, measured across lines A–A′ etc., varies as the western end of the SAFS is approached (see text for discussion). (b) Map and stereographic projections showing the complex variation in slip direction within the Perachora Fault Segment Boundary (after Morewood and Roberts, 1997). Circled numbers on the maps of (a) and (b) correspond to the stereographic projections.

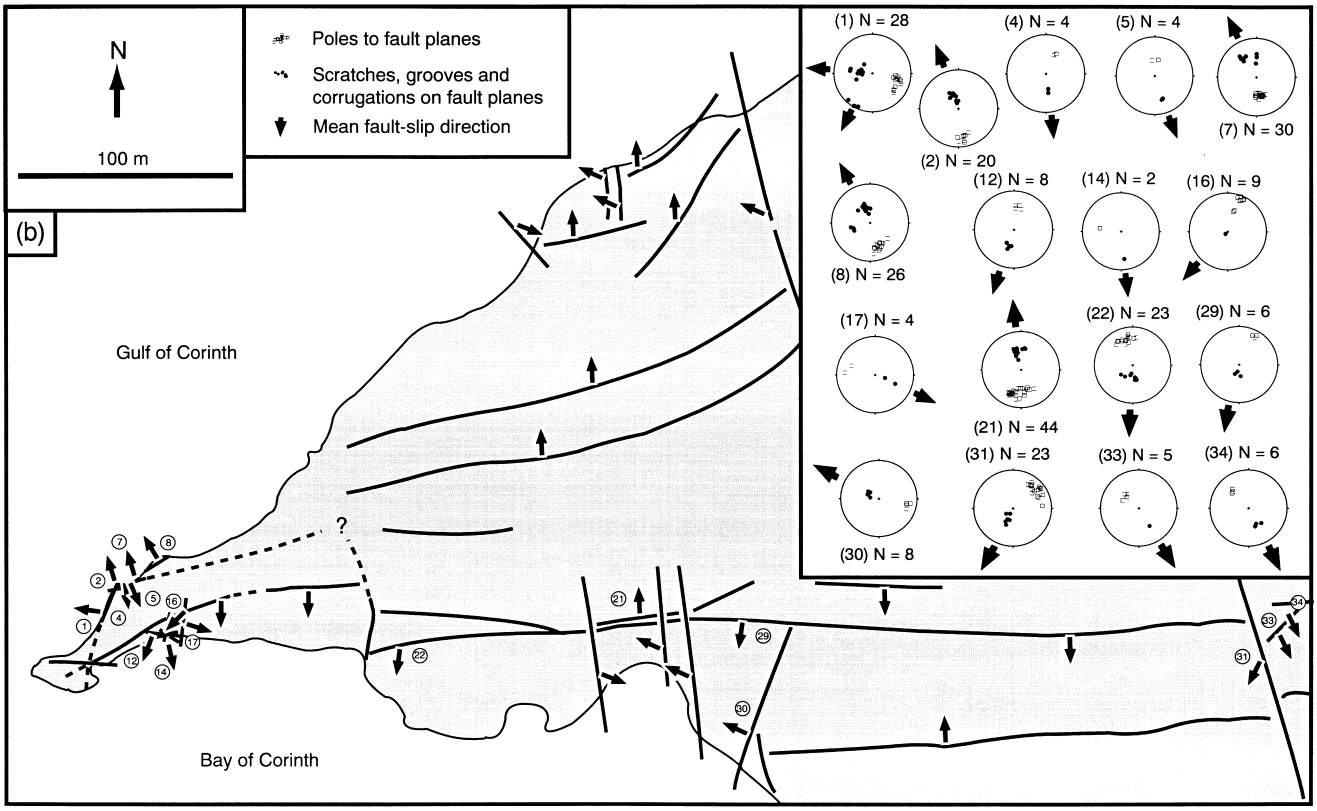


Fig. 3. (*continued*)

Gulf of Corinth. Several workers have described and interpreted the terraces which lie south of the Gulf of Lechaio and the Corinth Isthmus, in the footwall of the XFS (e.g. Vita-Finzi and King, 1985; Keraudren and Sorel, 1987; Collier, 1990; Doutsos and Piper, 1990; Collier et al., 1992; Armijo et al., 1996). Armijo et al. (1996) mapped 10 marine terraces and palaeoshorelines in this area and used them to estimate rates of deformation on the XFS. These authors correlated the Corinth terraces with late Pleistocene oxygen-isotope stages of sea-level highstands and hence with global sea-level fluctuations. This enabled them to describe uplift and flexure in the footwall of the XFS as a function of distance from the surface trace of the fault.

Previous mapping of the Perachora Peninsula has revealed so-called Tyrrhenian coastal deposits constituting terraces 10–20 m high overlying 20–30 m of deeper marine conglomerates, marls and sandstones of Upper Pliocene age (IGME, 1984). U-series dating of corals has yielded ages of $128 \pm 3$ ka for the marine terrace at 22 m elevation north of Heraion and $134 \pm 3$ ka for deposits at 26 m elevation 100 m east of the channel leading into Lake Vouliagmeni (Vita-Finzi, 1993) (VF 89/2 and VF 89/3, Fig. 4). However, our field studies have identified two other, higher and presumably older terraces. The Perachora Peninsula has been remapped using 1:25 000 topographic base maps with 20 m contour intervals to constrain the nature, geometries and elevations of the terraces. These results are described in the following sections and in Figs. 4 and 5.

### 3.2. Sedimentology

The marine deposits of the Quaternary terraces on the Perachora Peninsula comprise beach–shoreface sediments and/or algal bioherms overlying Upper Pliocene marls. At the western end of the Perachora Peninsula [Location (i), Figs. 4 and 5a] finely laminated Pliocene marls are unconformably overlain by up to a metre of lithophagid-bored marine cobbles. Above this, internally-laminated, domal-topped algal bioherms, incorporating marly-calc-arenaceous and bioclastic material, are observed up to several metres in height. A coarse, shelly sandstone, rich in marine fauna (corals, bivalves, gastropods, etc.) overlies the bioherms, infilling the spaces between the domal tops. This top layer, locally up to 1.2 m thick, provides the characteristic flat-topped appearance of the stepped marine terraces in this area (Morewood and Roberts, 1997). Supported by a U-series date of $128 \pm 3$ ka of a

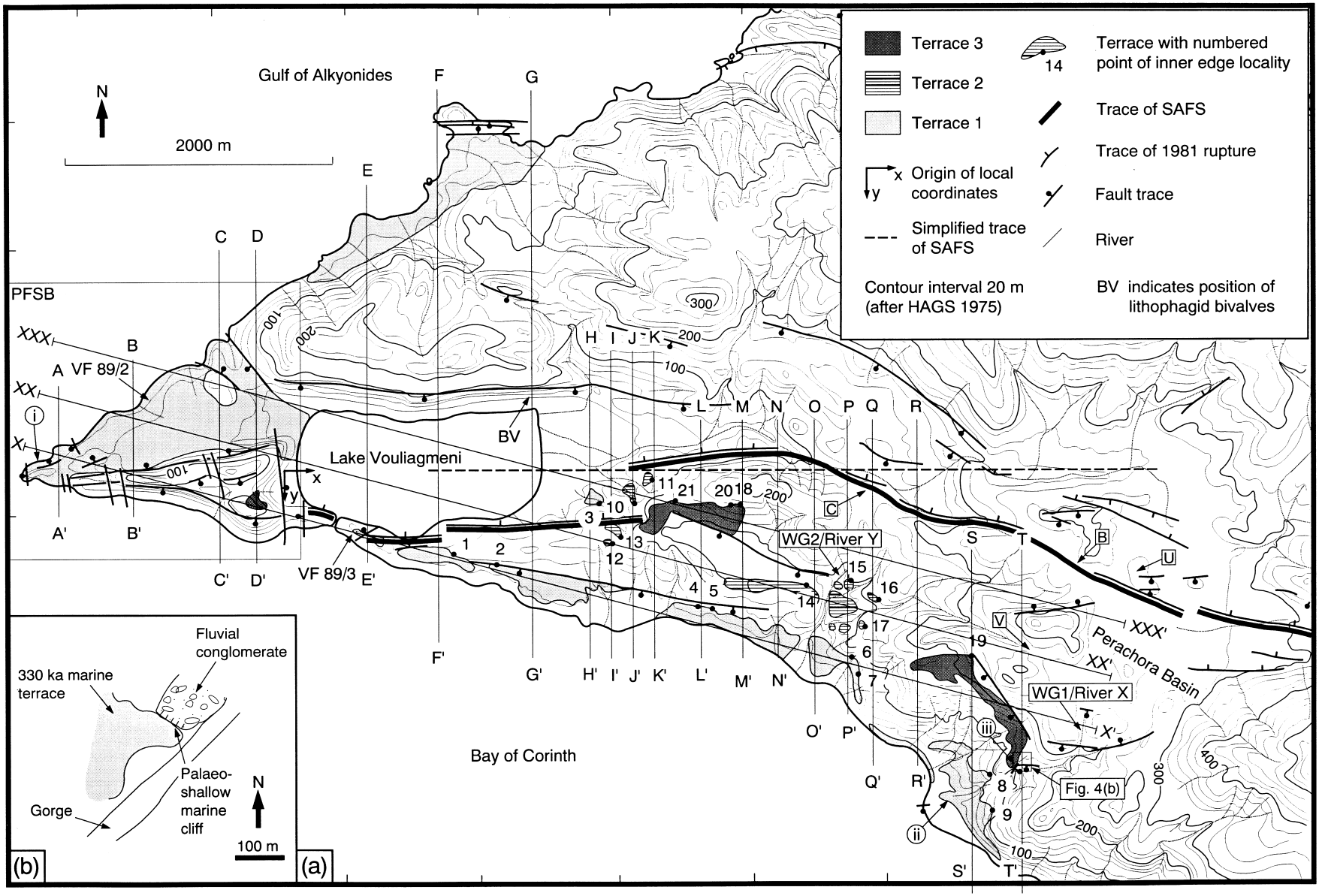


Fig. 4. (a) Map showing the location of raised marine terraces and the structure of the Perachora Peninsula. The present day surface expression of the western end of the South Alkyonides Fault Segment (SAFS) is defined by faults and surface ruptures (new mapping and after Jackson et al., 1982 and IGME, 1984). The complexly deformed area of the Perachora Fault Segment Boundary (PFSB), mainly west of Lake Vouliagmeni, consists of c. E–W and c. N–S faults (after Morewood and Roberts, 1997) (see also Fig. 3b). The origin of the coordinates given to the back points of the marine terraces is located at the position of the proposed end of the SAFS and the E–W dotted line is its simplified surface trace. Some logs shown in Fig. 5(a) are indicated by lower case Roman numerals. Positions of cross-sections shown in Fig. 5(b) are indicated by lines labelled with uppercase letters (e.g. A–A′). Positions of wind gaps referred to in the text are indicated (WG1 and WG2). Locations of dated corals are indicated as VF 89/2 and VF 89/3 (Vita-Finzi, 1993). (b) Sketch map of Locality (iii) showing the 330 ka marine terrace onlapping a palaeo-submarine cliff (see text for discussion).

coral (Vita-Finzi, 1993; VF 89/2, Fig. 4), we interpret these sediments as being beach–shoreface deposits that formed during the 125 ka sea-level highstand. Below, we correlate these sediments with other marine deposits that we have mapped along the southern shore of the Perachora Peninsula (Figs. 4 and 5).

We have also found evidence for higher and presumably older terraces. At location 11 (Fig. 4) a $>2.0$ m thick conglomerate (sub-rounded pebbles in a marl–calc-arenite matrix) is overlain by up to 20 cm of finely laminated algal mat. Marine gastropods are observed in the top few centimetres of the conglomerate and bound within the algal layer. A thin (3–5 cm) sandy unit, rich in marine fauna such as corals, bivalves and gastropods, covers the algal layer. At location 15 (Fig. 4) Pliocene marls are overlain by lithophagid-bored massive conglomerate units. Thick (up to 2.5 m) internally-laminated algal bioherms, incorporating marine material (whole and fragmented bivalves, corals, etc.) overlie the conglomerates. Submarine (?) channels comprising intensely lithophagid-bored pebbles locally incise the bioherms. At location 16 (Fig. 4) algal material is scarce and finely-laminated calc-arenites, rich in marine fauna, overlie the conglomerates. The marine sediments at locations 11, 15 and 16 are interpreted as beach–shoreface deposits which we argue below represents the 240 ka sea-level highstand.

The highest terrace is exposed at location (iii) (Figs. 4 and 5a). Here, marine sediments onlap fluvial deposits (angular clasts, no lithophagid borings), the implications of which are discussed in a later section of this paper. These marine sediments, at least 1.5 m thick, are dominated by intensely bored (lithophagid bivalves) rounded limestone cobbles in a sandy–shelly matrix. Importantly for our later discussion, the fluvial conglomerates here are composed of angular pebbles of chert, volcanic rocks and limestone. The marine deposits contain no chert or volcanic pebbles. The marine deposits at this location slope gently up landwards and are interpreted below as representing the 330 ka sea-level highstand.

### 3.3. Methodology

Twenty N–S cross-sections and three ESE–WNW cross-sections identify three distinct raised marine terraces (Fig. 5b). N–S cross-sections were used in order to measure the perpendicular distances of the inner edges of the marine terraces from the idealised trace of the SAFS to the north and from the proposed western end of the fault (see Fig. 4). ESE–WNW cross-sections were chosen in order to intersect as many different terraces as possible, thus enabling better along-strike correlation. Drainage is also marked on the map and cross-sections as this is important in our analysis of the evolution of the area (see below).

We have assigned local coordinates to the points of elevation estimates along the inner edges of the terraces that lie within the footwall of the SAFS (see below and Table 1). The origin of these local coordinates is close to the proposed termination of the present day surface trace of the western end of the SAFS (Fig. 4). This point was chosen because (i) the latest surface rupturing event in 1981 propagated to c. 100 m west of the channel connecting Lake Vouliagmeni and the Bay of Corinth (IGME, 1984); (ii) it is where the throw and geomorphic expression across the fault tends to zero (Fig. 3a). We measured $x$ coordinates parallel to the simplified surface trace of the western end of the SAFS, away from the end of the fault (Fig. 4); $y$ coordinates were measured perpendicular to this line. Inner edges of terraces were identified in the field and marked on the maps (numbers 1–21 in Fig. 4 and Table 1). The elevations of these points together with their local coordinates are shown in Table 1. At worst, the horizontal mislocation of the inner edges of the terraces is 100 m (e.g. in places where erosion has caused landward retreat of the cliff and/or degradation of the terrace deposits). Where the terrace–palaeo-sea-cliff contact is exposed in the field (e.g. Point 8, Fig. 4 and Table 1) the horizontal mislocation of the inner edges is $<100$ m (i.e. less than twice the size of the dots indicating the positions of inner edges in Fig. 4). Elevation estimates are accurate to $\pm 5$ m for the youngest (125 ka) terrace and $\pm 10$ m for the 240 and 330 ka terraces. These errors are shown on the appropriate graphs (see later in Figs. 7, 8a and 9a).

### 3.4. Correlation of the marine terraces with sea-level highstands

As described above, the stepped marine terraces in the Gulf of Corinth represent Pleistocene sea-level highstands (Armijo et al., 1996). Fig. 6 shows the absolute sea-level fluctuation over the past 340 ka, derived mainly from raised coral reefs on the Huon Peninsula, Papua New Guinea (Chappell and Shackleton, 1986; Merritts and Bull, 1989). Other workers have used this sea-level curve in the Gulf of Corinth (e.g. Keraudren and Sorel, 1987; Collier, 1990; Armijo et al., 1996) and elsewhere (e.g. Merritts and Bull, 1989). We have distinguished three different marine terraces on the southern shores of the Perachora Peninsula (Fig. 4). Terrace 1 (Fig. 4) is the most continuous of the mapped terraces and is therefore likely to correspond to a prominent highstand (see above). We correlate Terrace 1 with the 125 ka sea-level highstand. This is consistent with U-series dates of $128 \pm 3$ and $134 \pm 3$ ka (Vita-Finzi, 1993) and perhaps with the work of Dia et al. (1997). This correlation gives uplift rates that can be used as guidelines in correlating the other terraces to sea-level highstands. Assuming a

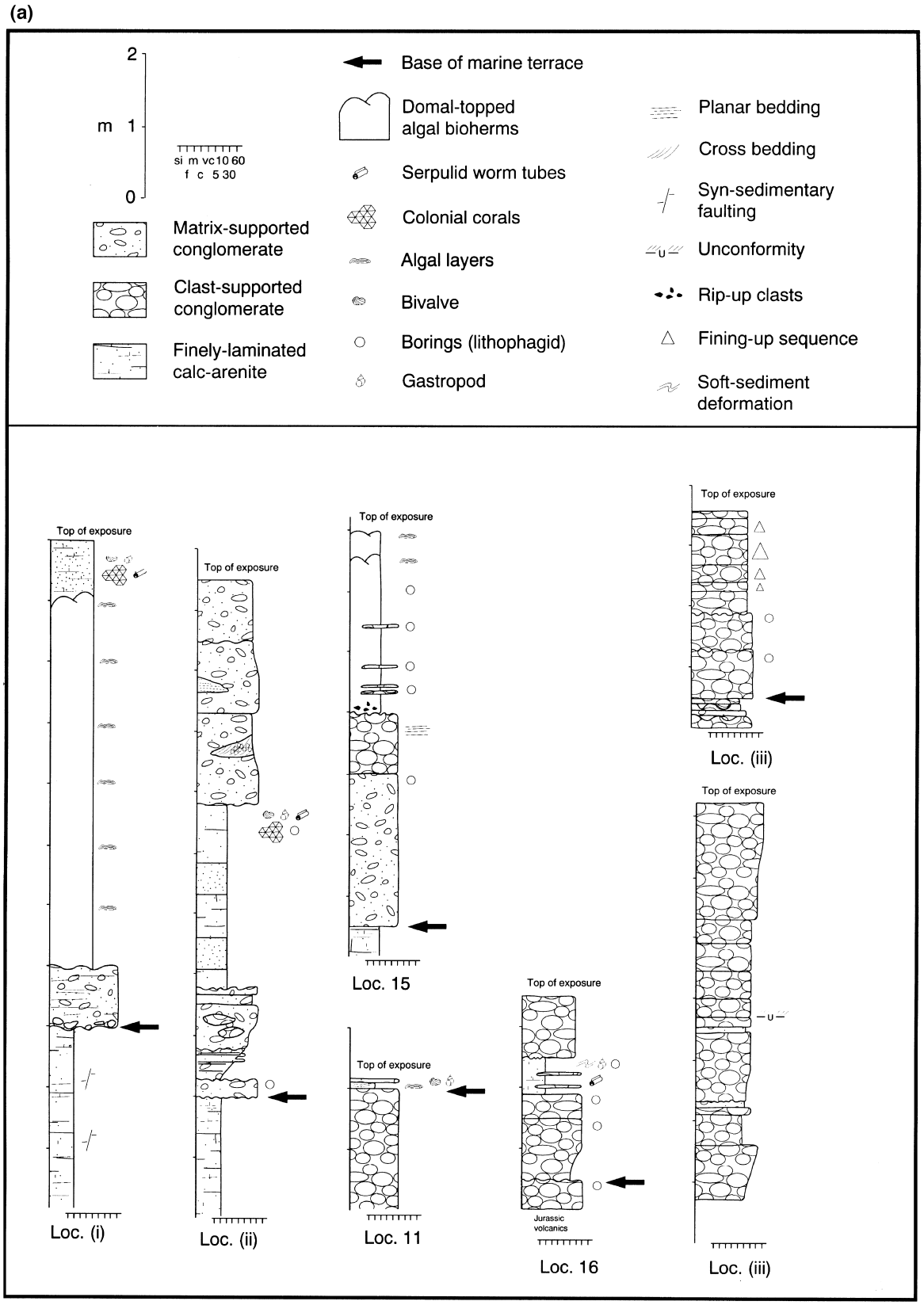


Fig. 5. (a) Graphic logs (located in Fig. 4) showing the sedimentology of the raised marine terraces and fluvial deposits referred to in the text. (b) Cross-sections (located in Fig. 4) showing the positions of raised marine terraces and the structure of the Perachora Peninsula. The position of the SAFS in each section is highlighted. Note the difference in scales between the WNW–ESE and the N–S sections and the vertical exaggerations of ×7.5 and ×3.5, respectively.

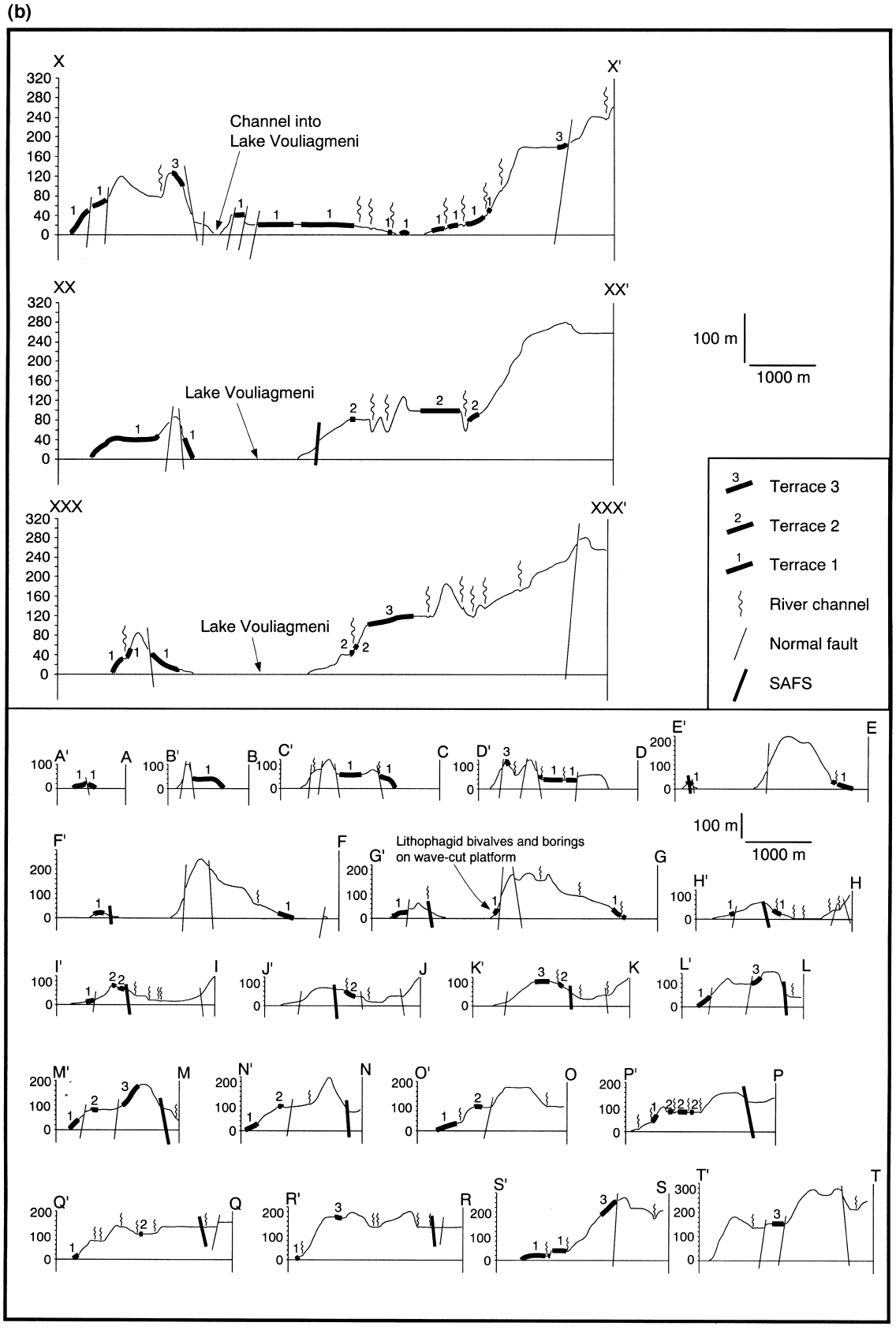


Fig. 5. (*continued*)

Table 1
Local coordinates ($x$,$y$), elevations ($z$) and uplift rates of points along the inner edges of the three raised marine terraces on the Perachora Peninsula. Origin of the local coordinates and positions of the numbered points are located in Fig. 4. A discussion of the errors involved is given in the text[a]

| Point No. | $x$ (m) | $y$ (m) | $z$ (m) | Uplift rate (mm/y) |
|---|---|---|---|---|
| *Terrace 1* | | | | |
| 1 | 1285 | 643 | 35 | 0.28 |
| 2 | 1607 | 714 | 35 | 0.28 |
| 3 | 2178 | 250 | 40 | 0.32 |
| 4 | 3088 | 1053 | 40 | 0.32 |
| 5 | 3213 | 1071 | 40 | 0.32 |
| 6 | 4213 | 1464 | 60 | 0.48 |
| 7 | 4284 | 1607 | 60 | 0.48 |
| 8 | 5302 | 2321 | 80 | 0.64 |
| 9 | 5319 | 2624 | 80 | 0.64 |
| *Terrace 2* | | | | |
| 10 | 2642 | 250 | 80 | 0.33 |
| 11 | 2749 | 89 | 80 | 0.33 |
| 12 | 2481 | 553 | 80 | 0.33 |
| 13 | 2535 | 500 | 80 | 0.33 |
| 14 | 3927 | 893 | 100 | 0.42 |
| 15 | 4248 | 875 | 100 | 0.42 |
| 16 | 4463 | 1018 | 110 | 0.46 |
| 17 | 4355 | 1232 | 120 | 0.5 |
| *Terrace 3* | | | | |
| 18 | 3427 | 268 | 170 | 0.52 |
| 19 | 5141 | 1464 | 245 | 0.74 |
| 20 | 3345 | 266 | 160 | 0.49 |
| 21 | 2938 | 230 | 120 | 0.36 |

[a] Errors for $x$ and $y$ are less than $\pm$100 m; $z$ is accurate to $\pm$5 m for Terrace 1 and $\pm$10 m for Terraces 2 and 3; errors in uplift rate are $\pm$0.04 mm/y for Terraces 1 and 2 and $\pm$0.03 mm/y for Terrace 3. See text for full discussion.

nearly constant uplift rate at any one locality along the palaeo-shorelines (see Lajoie, 1986; Merritts and Bull, 1989; Armijo et al., 1996) we correlate Terraces 2 and 3 with the sea-level highstands at 240 and 330 ka, respectively (Fig. 6). In agreement with the constant uplift rate hypothesis we prefer to correlate Terrace 2 with the 240 ka highstand but do not discount the possibilities of correlation with highstands at 210 and 200 ka (Fig. 6). We are confident that Terrace 3 corresponds to the 330 ka highstand as it is unlikely that the lower highstands at 300 and 280 ka (Fig. 6) would have overprinted the 330 ka sediments. If uplift rates are constant at a single locality then Fig. 7 (elevation plotted as a function of terrace age at a particular point along the coastline) is consistent with our interpreted terrace ages. This is because the ages are nearly equidistant in time and would show a linear relationship with elevation.

### 3.5. Deformation of the marine terraces

Elevations of the inner edges (points 1–21, Fig. 4 and Table 1) have been plotted against distance from

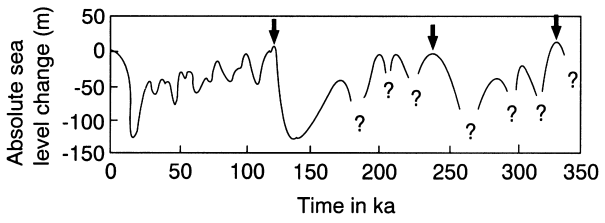


Fig. 6. Absolute sea-level fluctuation (data from Chappell and Shackleton, 1986; Merritts and Bull, 1989) with 125, 240 and 330 ka highstands indicated by the black arrows.

the proposed end of the SAFS for each separate terrace. These plots (Fig. 8a) represent the present day profile of each terrace within the footwall of the most western 5.5 km of the SAFS. They show that cumulative uplift decreases towards the lateral termination of the fault. If viewed in terms of a simple tilt, the profiles indicate a difference in elevation of 45 m (80 − 35 m) over c. 4 km for Terrace 1, 40 m (120 − 80 m) over c. 3 km for Terrace 2 and 125 m (245 − 120 m) over c. 1.5 km for Terrace 3. These data give angles of tilt towards the fault termination of 0.78° for Terrace 1, 1.22° for Terrace 2 and 3.25° for Terrace 3. Thus, the older terraces are more tilted because they have been subjected to more cumulative deformation. However, to regard the profiles as a simple tilt may be an oversimplification. The best-fit lines through the data for all three terraces are exponential functions and we have plotted these on Fig. 8(a). However, a linear function fits the data reasonably well and we do not discount this possibility. Either way, the implications for fault growth presented in this paper do not change. The exponential functions produce concave-upward profiles reminiscent of the bell-shaped (displacement–distance) curves of some fault growth models (e.g. Cowie and Scholz, 1992a,b,c) (Fig. 8b) whilst the linear functions are consistent with other fault growth models (e.g. Cowie and Shipton, 1998).

### 3.6. Uplift rates

With the above knowledge of the shapes and ages of marine terraces on the Perachora Peninsula, we have calculated the spatial variation in uplift rates at the end of the SAFS. Assuming an age of 125 ka for Terrace 1 (see above discussion), uplift rates for this terrace averaged over the last 125 ka are from 0.28 $\pm$ 0.04 mm/y [Point 1 (Fig. 4 and Table 1), present elevation 35 m] to 0.64 $\pm$ 0.04 mm/y (Point 9, present elevation 80 m). Similarly, uplift rates averaged over the last 240 ka for Terrace 2 range between 0.33 $\pm$ 0.04 mm/y (Point 10, present elevation 80 m) and 0.50 $\pm$ 0.04 mm/y (Point 17, present elevation 120 m) and over the last 330 ka for Terrace 3 range between 0.36 $\pm$

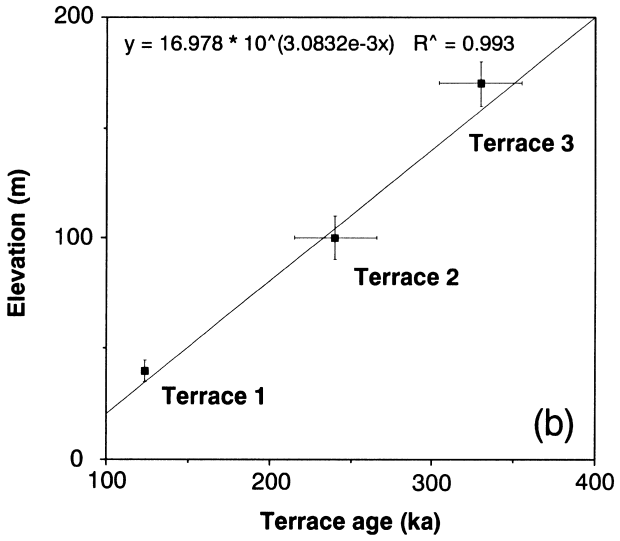


Fig. 7. Elevation against estimated age for Terraces 1, 2 and 3 along line M–M′ (located in Fig. 4). The good linear correlation implies a near constant uplift rate within the footwall of the western end of the SAFS over the last 330 ka. See text for discussion.

0.03 mm/y (Point 21, present elevation 120 m) and 0.74 ±0.03 mm/y (Point 19, present elevation 245 m).

Contrary to our earlier assumption, the wider spacing of the best-fit lines for Terraces 2 and 3 compared to Terraces 1 and 2 implies that uplift rates have been similar over time for Terraces 1 and 2 but perhaps slightly higher for Terrace 3 (Fig. 8a). In order to investigate how uplift rate has varied over the last 330, 240 and 125 ka we have plotted uplift rate as a function of distance from the end of the SAFS (Fig. 9a). This plot shows very similar curves for Terraces 1 and 2, implying that, at a given point along the SAFS, uplift rate has been similar when averaged over 125 or 240 ka. However, the curve for Terrace 3 appears to indicate higher uplift rates, especially towards the centre of the SAFS, but it is important to note that the rate is averaged over a longer time period, that is 330 ka. This implies that uplift rates were higher between 330 and 240 ka than from 240 ka to the present day. If (1) the higher uplift rates for the 330 ka are real and not an artefact of only four data points, or (2) rates have been constant with time, our observations are inconsistent with a tip propagating at depth producing lateral migration of uplift (Fig. 9b). This would produce uplift rates which increase with time at any one point along the coastline (Fig. 9b). We will discuss this further below.

## 4. Deformed drainage on the Perachora Peninsula

The marine terraces described above can be used to date times when drainage channels on the Perachora Peninsula were being cut by the growing SAFS and allow us to calculate a propagation rate for its surface trace.

Prominent wind gaps in the footwall of the SAFS indicate the former courses of drainage channels that flowed across what is now the surface expression of the fault (Fig. 4). These wind gaps take the form of incised gorges through Triassic–Jurassic limestone and Jurassic volcanics, with fluvial deposits preserved in places along their sides. Fig. 4(b) shows fluvial con-

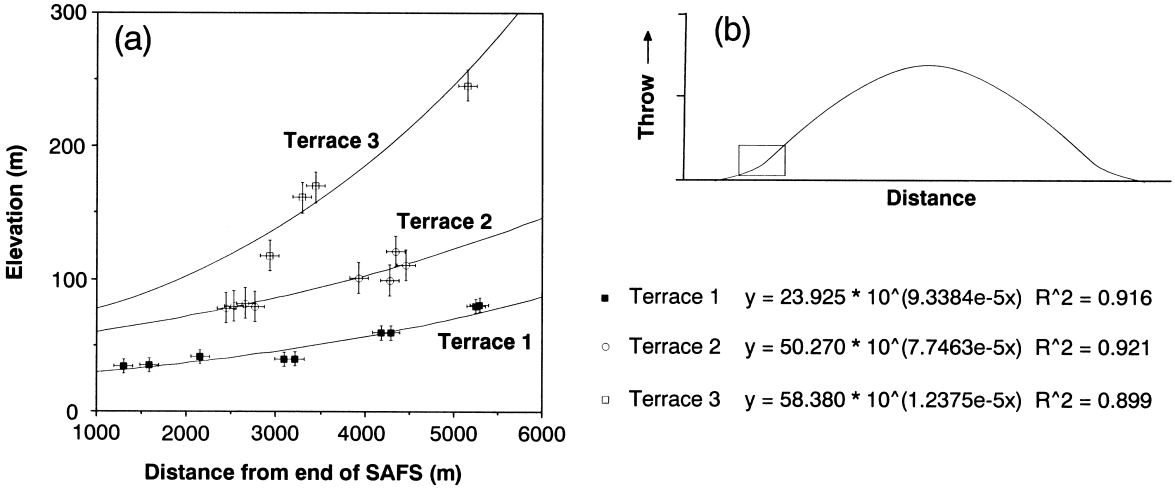


Fig. 8. (a) Elevation against distance east from the proposed end of the SAFS for the back points of the three raised marine terraces on the Perachora Peninsula (see Fig. 4). The plots show a concave-upwards profile of footwall deformation along-strike of the SAFS with uplift decreasing towards the PFSB. The profiles are similar to the part of the bell-shaped throw–distance curve shown in (b). See text for discussion.

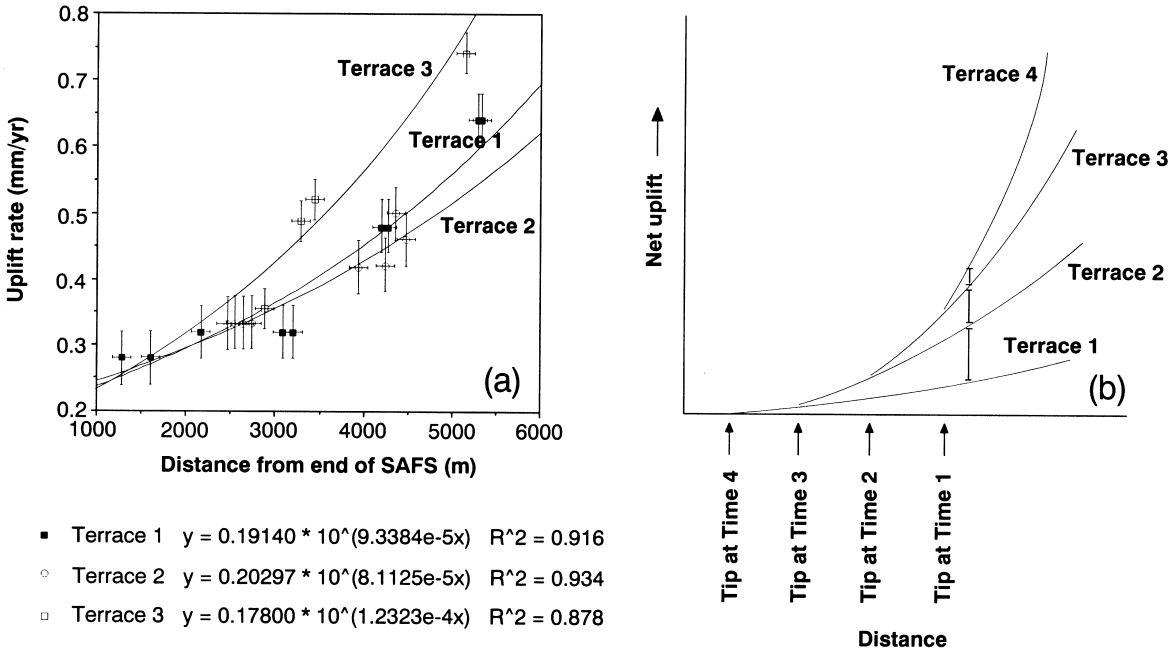


Fig. 9. (a) Uplift rate plotted as a function of distance east from the proposed end of the SAFS for Terraces 1, 2 and 3. (b) Schematic plot of cumulative uplift for four terraces (T1 = youngest, T4 = oldest) spaced at equal time intervals lying in the footwall of a fault which is laterally propagating at depth at a constant rate. The uplift rate at any one point (indicated by vertical bars) has increased with time, i.e. more uplift occurred between Terrace 1 and Terrace 2 than between Terrace 3 and Terrace 4. See text for discussion.

glomerates which form a palaeo-submarine cliff that has been eroded into, and onlapped by the 330 ka marine terrace (Fig. 10). The fluvial conglomerates are composed of angular clasts of chert and volcanics; the marine conglomerates are dominated by rounded, lithophagid-bored limestone cobbles and contain no chert or volcanics. The fluvial sediments therefore predate the marine terrace deposits. We propose that this river (X, Figs. 4 and 11) was beheaded by the propagating SAFS prior to the 330 ka sea-level highstand. So, the tip of the fault has propagated from west of the position of the river X to the western end of Lake Vouliagmeni (Figs. 4 and 11). The question is where exactly was the tip at 330 ka? If we can constrain this we can derive a rate of lateral propagation. The tip must have been west of the drainage divide at V (Fig. 4) at 330 ka otherwise river X could have flowed around the western side of hill U (Fig. 4) and entered the gorge containing the fluvial conglomerates (WG1, Fig. 4). It did not, so the easternmost possible position of the tip was at point B (Figs. 4 and 11b). Point B is c. 5.5 km from the present lateral surface termination of the fault at the western end of Lake Vouliagmeni (Fig. 4). The course of river Y was submarine at 330 ka (Fig. 11b). Incision of river Y must have occurred after 330 ka but prior to the river being beheaded by the propagating fault at c. 240 ka (Fig. 11). This suggests a westernmost position for the tip of the SAFS at 330 ka (Point C, Fig. 11), c. 4 km from its present day termination (Figs. 4 and 11f). As discussed earlier, we believe the present day position of the westernmost extent of the surface trace of the SAFS to be reasonably well constrained and assign an error of 500 m to the east. Therefore, the propagation rate since 330 ka has been 12.1–16.7 mm/y.

Below we use the propagation rate (16.7 mm/y) for the surface expression of the tip of the SAFS to reconstruct the palaeogeography of the Perachora Peninsula at 345, 330, 270, 240, and 125 ka and explain the formation of the two wind gaps (WG1 and WG2) shown on Fig. 4.

### *4.1. 345 ka palaeogeography (Fig. 11a)*

Working back from 345 ka, using the 16.7 mm/y propagation rate in conjunction with topographic data (HAGS, 1975) and the sea-level curve (Fig. 6), we have reconstructed the palaeogeography of the Perachora Peninsula at the 345 ka sea-level lowstand. The tip of the surface trace of the SAFS would have been at position A. Drainage flowing from the higher hanging wall topography in the north had probably been beheaded by this time by the propagating SAFS, forming a wind gap in its footwall (WG1, Figs. 4 and 11).

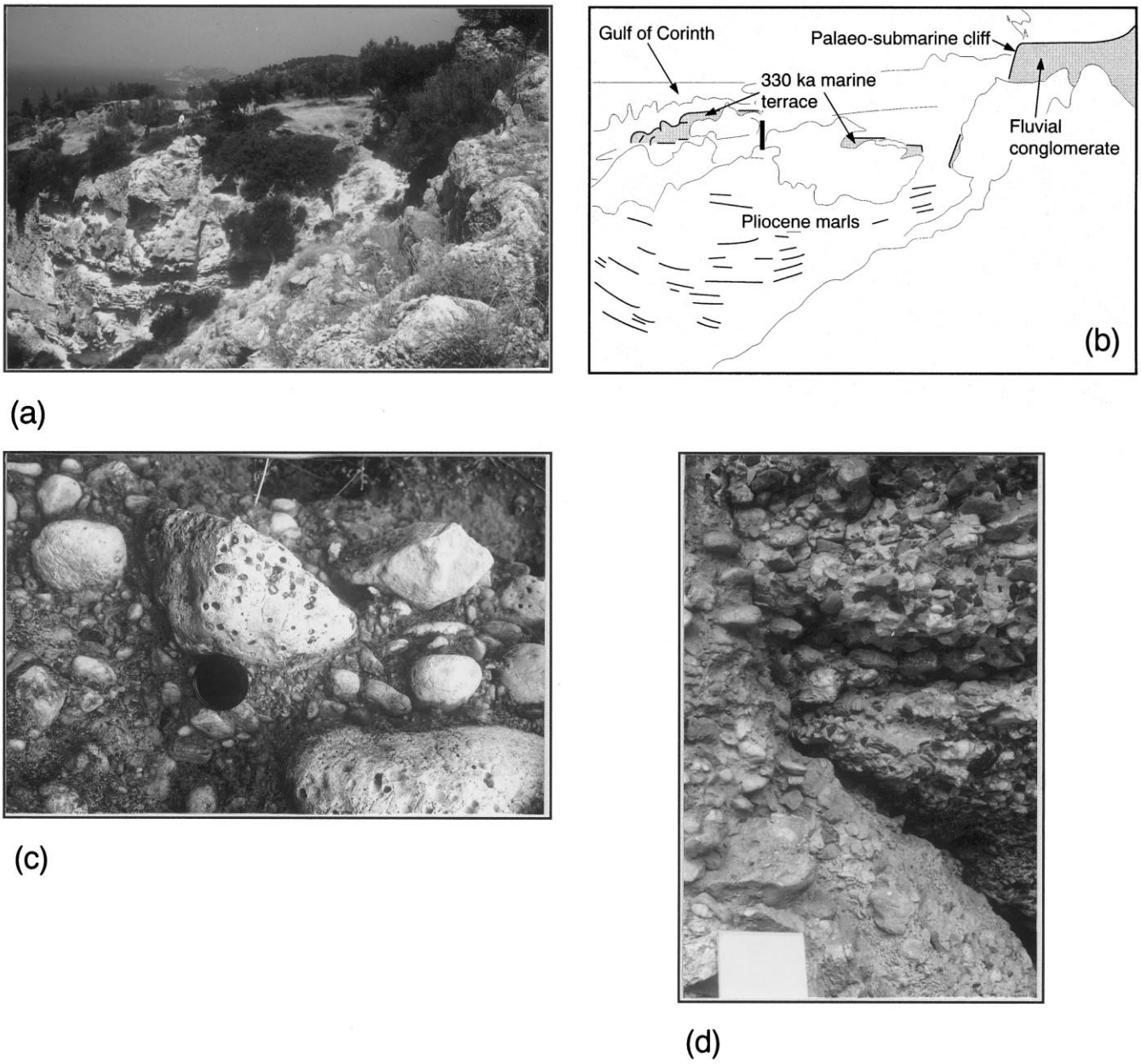


Fig. 10. (a) Photograph and (b) interpretative sketch showing the sediments of the 330 ka marine terrace (Terrace 3) onlapping a palaeo-submarine cliff composed of fluvial deposits. Pliocene marls underlie the marine deposits. The fluvial deposits predate the 330 ka terrace. Drainage to this area is proposed to have been cut off by propagation of the surface trace of the SAFS prior to 330 ka (see text for discussion). (c) Marine conglomerate intensely bored by lithophagid bivalves. (d) Angular fluvial conglomerate forming the palaeo-submarine cliff.

### *4.2. 330 ka palaeogeography (Fig. 11b)*

As described above, the tip of the surface expression of the SAFS would have reached position B by 330 ka. Drainage from the north, which had previously run to enter the sea via a river (X), was directed westwards, along-strike of the fault and around its tip (River Y).

### *4.3. 270 ka palaeogeography (Fig. 11c)*

Assuming the 16.7 mm/y propagation rate derived above, at 270 ka the tip would have been at position C such that river Y was still able to flow west and then south around it towards the coastline, cutting a gorge in the underlying bedrock.

### *4.4. 240 ka palaeogeography (Fig. 11d)*

By 240 ka propagation of surface trace of the SAFS would have reached position D. This would have caused the abandonment of river Y, forming a second wind gap (WG2, Figs. 4 and 11d). All the drainage

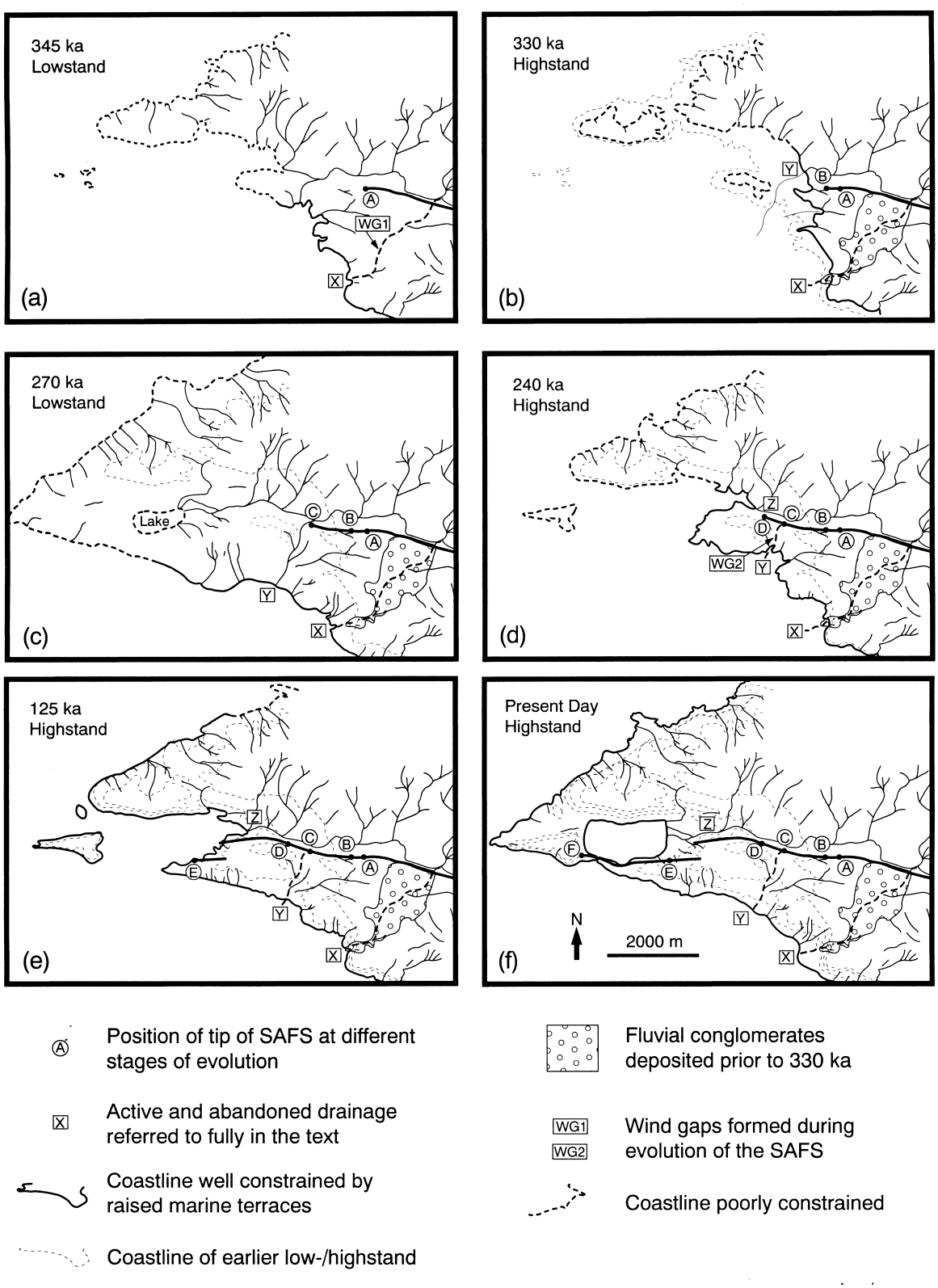


Fig. 11. Evolution of the Perachora Peninsula since 345 ka assuming a rate of 16.7 mm/y for the propagation of the surface trace of the South Alkyonides Fault Segment (SAFS). The coastline at (a) 345 ka, (b) 330 ka, (c) 270 ka, (d) 240 ka, (e) 125 ka and (f) the present day are shown by medium solid lines. Previous coastlines are shown by thin dashed lines. The surface trace of the SAFS is shown by a thick solid line with solid circles indicating the position of its tip at different times. Drainage which is proposed to have been cut off by the surface propagation of the SAFS is indicated by bold dashed lines; other drainage is shown by thinner solid lines. Letters refer to fault-tip positions and drainage described fully in the text.

from the hills to the north was gathered into an axially-flowing system (Z) which ran westwards to the sea.

### 4.5. 125 ka palaeogeography (Fig. 11e)

Between 240 and 125 ka, continued propagation of the SAFS at 16.7 mm/y would have caused drainage to flow axially to the west, via river Z. During this period, a transfer zone geometry formed, stepping the surface trace of the fault ~400 m to the south. We do not know whether this geometry continues to depth or whether the faults near the surface are splays linked to one main fault plane. However, it is interesting to note that such a feature can form in c. 115 ka. By 125 ka the end of the surface trace of the fault had reached position E. Associated evolution of the coastline further developed an E–W-trending bay, sheltered by a promontory of footwall uplift to the south and an emerging island to the west.

### 4.6. Present day palaeogeography (Fig. 11f)

Continued propagation at a rate of 16.7 mm/y between 125 ka and the present day has resulted in the end of the surface trace of the SAFS reaching position F. During this time, the emerging footwall has isolated a bay from the sea, forming an inland lake. Lake Vouliagmeni now lies in the immediate hanging wall of the SAFS and is divided from the Bay of Corinth by a small footwall uplift along its southern shore (Figs. 4 and 11f).

## 5. Discussion

Through the analysis of drainage on the Perachora Peninsula, we have shown that the tip-point of the SAFS propagated westwards over at least the past 330 ka in tandem with increasing footwall uplift and hence displacement. This observation is at first sight consistent with the hypothesis that fault displacement scales with length (e.g. Walsh and Watterson, 1988; Cowie and Scholz, 1992c). In order to test this hypothesis, we have examined the kinematics along the strike of the fault. Many models of fault growth require a damage zone at the propagating tip (see Cowie and Shipton, 1998 and references therein). The PFSB (Figs. 2–4) is a complexly deformed zone of cross-faulting and varied kinematics at the western end of the SAFS (Morewood and Roberts, 1997). If the PFSB is an example of a damage zone, and if the SAFS has been propagating laterally during growth, we should expect to see a trail of palaeo-segment boundary structures such as within the PFSB along-strike of the fault. In other words, if a zone of complex deformation immediately precedes the propagating tip of a fault we should expect to see these relic structures preserved along the fault trace. Fig. 3(a) shows the faulting pattern and kinematics along the SAFS. There are no N–S-striking faults along the SAFS east of the PFSB, and the fault-slip directions show a simple converging pattern of slip. No complex along-strike extension or oblate vertical flattening can be found along the trace of the SAFS in locations where the above drainage analysis suggests the tip would have been at any time over the last c. 345 ka (Fig. 11).

In order to explain these observations we invoke a model for fault growth which has the ends of the SAFS at depth fixed over at least the last c. 330 ka. In this model the throw–length profiles steepen with time as displacement is accumulated on the fault (Fig. 12). We suggest that oblate vertical flattening only occurs at the ends of the surface trace of the fault above where the tip is at depth. This model explains the absence of relic segment boundary structures and propagation of the surface trace of the fault without changing the length of the fault at depth (Fig. 12). If the fault was propagating laterally at depth then the uplift rate at any one point in the footwall would increase with time (Fig. 9b). We have presented results that imply that uplift rates at any one point in the footwall of the SAFS have either remained constant with time or decreased over the period 330–240 ka (Figs. 7 and 9a). The model presented in Fig. 12 is consistent with our observations of the deformed marine terraces in the footwall of the SAFS.

Constant uplift rate across a normal fault implies constant displacement rate across the same fault. Nicol et al. (1997) state that a fault with constant displacement rate will accommodate progressively more of the regional strain rate as its dimensions increase; that is, the rate of seismic moment on a growing fault increases even when the displacement rate is constant. These authors conclude that a "constant regional strain rate can be accommodated either by establishing fault lengths at early stages of growth of the system and slowing lateral propagation by fault interaction, or by decreasing the number of active faults with time, probably by the inactivation of smaller faults". Our results are consistent with the former scenario but do not exclude the latter. The model presented in Fig. 12 implies that, at least over the 330 ka time period considered here, values for the displacement–length ratio have increased with progressive deformation; that is, growth is not self-similar. The fixed position of the western end of the SAFS and the increasing displacement–length ratio with time may be due to interaction with the XFS (Fig. 2), perhaps in the manner described by Nicol et al. (1996). This is consistent with the idea that mechanical interaction is a major control

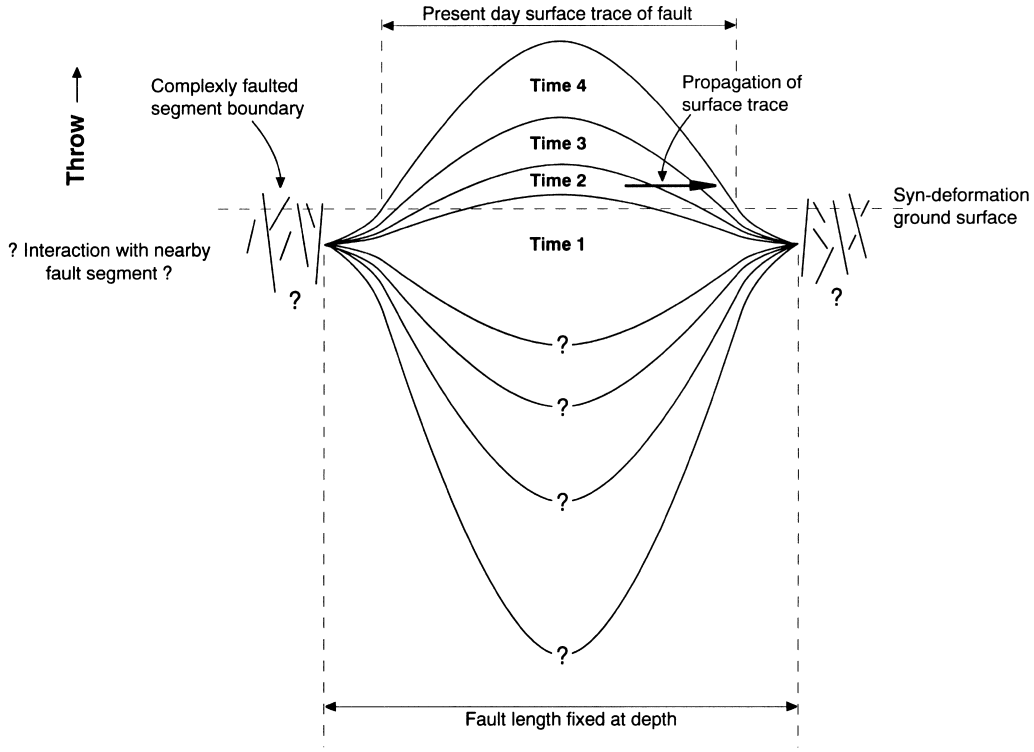


Fig. 12. Growth model for a fault with its end points effectively fixed over that time period. Note that each profile is the net result of many non-characteristic events (Roberts, 1996b) along the fault; it is not implied that the whole length of the fault has ruptured in any single event. This model allows propagation of the surface trace of the fault without an overall increase in length. Complexly deformed segment boundaries occur only at the ends of the fault. See text for discussion.

on displacement–length ratios during the growth of fault systems (Cowie, 1998).

## 6. Conclusions

1. Detailed mapping of deformed marine terraces and drainage on the Perachora Peninsula has provided insights into fault growth.
2. Ages have been inferred which correlate the terraces with sea-level highstands.
3. Uplift rates of three marine terraces in the footwall of the SAFS decrease towards the end of the fault. Over a distance of 3–4 km, these rates range from 0.28 to 0.64 mm/y for the 125 ka terrace, from 0.33 to 0.50 mm/y for the 240 ka terrace, and from 0.36 to 0.74 mm/y for the 330 ka terrace.
4. Plots of elevation against distance from the end of the fault for the inner edges of these terraces may exhibit a concave-upwards profile, similar to the bell-shaped displacement–length profiles of some fault growth models or a linear profile similar to other models.
5. Observations of drainage cut-off by the propagating fault have enabled us to estimate a propagation rate for the surface trace of the SAFS of 12.1–16.7 mm/y. We have used this information to describe the structural and geomorphological evolution of the Perachora Peninsula over the last 345 ka.
6. The lack of a trail of segment boundary structures, similar to that documented by Morewood and Roberts (1997), along the SAFS implies a non self-similar growth model, in which the ends of the fault at depth are effectively fixed over the period we consider (330 ka). Surface propagation of the fault is due to values for the displacement–length ratio of the fault increasing with time. It is unlikely that such processes are unique to the SAFS and we would expect them to describe the growth of other active normal faults in the Gulf of Corinth and perhaps regions of active extension worldwide.

## Acknowledgements

This study was funded by a Birkbeck College Research Scholarship (NCM) and NERC GR9/1034

and GR9/02995 and Birkbeck College (GPR). IGME are thanked for permission to conduct fieldwork. The Benfield Greig Hazard Research Centre is thanked for support. Lee Anderson, Simon Baker, Mike Beling, Phil MacMurdie, Steven Miners and Andrew Reynolds are thanked for assistance and discussion in the field. Andrew Nicol and Iain Stewart provided thorough reviews which improved the manuscript.

## References

Abercrombie, R., Main, I.G., Douglas, A., Burton, P.W., 1995. The nucleation and rupture process of the 1981 Gulf of Corinth earthquakes from deconvolved broad-band data. Geophysical Journal International 120, 393–405.

Ambraseys, N.N., Jackson, J.A., 1990. Seismicity and associated strain of central Greece between 1890 and 1988. Geophysical Journal International 101, 663–708.

Armijo, R., Meyer, B., King, G.C.P., Rigo, A., Papanastassiou, D., 1996. Quaternary evolution of the Corinth Rift and its implications for the Late Cenozoic evolution of the Aegean. Geophysical Journal International 126, 11–53.

Billiris, H., Paradissis, G., England, P., Featherstone, W., Parsons, B., Cross, P., Rands, P., Rayson, M., Sellers, P., Ashkenazi, V., Davison, M., Jackson, J., Ambraseys, N., 1991. Geodetic determination of tectonic deformation in central Greece from 1900 to 1988. Nature 350, 124–129.

Chappell, J., 1974. Geology of coral terraces, Huon Peninsula, New Guinea: A study of tectonic movements and sea-level changes. Geological Society of America Bulletin 85, 553–570.

Chappell, J., Shackleton, N.J., 1986. Oxygen isotopes and sea level changes. Nature 324, 137–140.

Collier, R.E.Ll., 1990. Eustatic and tectonic controls upon Quaternary coastal sedimentation in the Corinth Basin, Greece. Journal of the Geological Society of London 147, 301–314.

Collier, R.E.Ll., Leeder, M.R., Rowe, R.J., Atkinson, T.C., 1992. Rates of tectonic uplift in the Corinth and Megara basins, Central Greece. Tectonics 11, 1159–1167.

Cowie, P.A., 1998. A healing–reloading feedback control on the growth rate of seismogenic faults. Journal of Structural Geology 20, 1075–1087.

Cowie, P.A., Scholz, C.H., 1992a. Growth of faults by accumulation of seismic slip. Journal of Geophysical Research 97, 11085–11095.

Cowie, P.A., Scholz, C.H., 1992b. Physical explanation for the displacement–length relationship of faults using a post-yield fracture mechanics model. Journal of Structural Geology 14, 1133–1148.

Cowie, P.A., Scholz, C.H., 1992c. Displacement–length scaling relationship for faults: data synthesis and discussion. Journal of Structural Geology 14, 1149–1156.

Cowie, P.A., Shipton, Z.K., 1998. Fault tip displacement gradients and process zone dimensions. Journal of Structural Geology 20, 983–997.

Dia, A.N., Cohen, A.S., O'Nions, R.K., Jackson, J.A., 1997. Rates of uplift investigated through $^{230}$Th dating in the Gulf of Corinth (Greece). Chemical Geology 138, 171–184.

Doutsos, T., Piper, D.J.W., 1990. Listric faulting, sedimentation, and morphological evolution of the Quaternary eastern Corinth rift, Greece: First stages of continental rifting. Geological Society of America Bulletin 102, 812–829.

Gawthorpe, R.L., Sharp, I., Underhill, J.R., Gupta, S., 1997. Linked sequence stratigraphic and structural evolution of propagating normal faults. Geology 25, 795–798.

HAGS (Hellenic Army Geographical Service), 1975. Topographical map of Perachora, Greece, scale 1:50,000.

Hubert, A., King, G.C.P., Armijo, R., Meyer, B., Papanastassiou, D., 1996. Fault reactivation, stress interaction and rupture propagation in the 1981 Corinth earthquake sequence. Earth and Planetary Science Letters 142, 573–585.

IGME (Institute of Geology and Mineral Exploration), 1984. Geological map of Greece, Perachora sheet, scale 1:50,000.

Jackson, J.A., Leeder, M.R., 1994. Drainage systems and the development of normal faults: an example from Pleasant Valley, Nevada. Journal of Structural Geology 16, 1041–1061.

Jackson, J.A., Gagnepain, J., Houseman, G., King, G.C.P., Papadimitriou, P., Soufleris, C., Virieux, J., 1982. Seismicity, normal faulting, and the geomorphological development of the Gulf of Corinth (Greece): The Corinth earthquakes of February and March 1981. Earth and Planetary Science Letters 57, 377–397.

Jackson, J.A., Norris, R., Youngson, J., 1996. The structural evolution of active fault and fold systems in central Otago, New Zealand: evidence revealed by drainage patterns. Journal of Structural Geology 18, 217–234.

Keraudren, B., Sorel, D., 1987. The terraces of Corinth (Greece)—a detailed record of eustatic sea-level variations during the last 500,000 years. Marine Geology 77, 99–107.

Lajoie, K.R., 1986. Coastal tectonics. In: Active Tectonics. National Academic Press, Washington, DC, pp. 95–124.

Merritts, D., Bull, W.B., 1989. Interpreting Quaternary uplift rates at the Mendocino triple junction, northern California, from uplifted marine terraces. Geology 17, 1020–1024.

Morewood, N.C., Roberts, G.P., 1997. The geometry, kinematics and rates of deformation in a normal fault segment boundary, central Greece. Geophysical Research Letters 24, 3081–3084.

Myrianthis, M.L., 1982. Geophysical study of the epicentral area of the Alkyonides Islands Earthquakes, central Greece. Geophysical Institute of Hungary. Geophysical Transactions 28, 5–17.

Nicol, A., Watterson, J., Walsh, J.J., Childs, C., 1996. The shapes, major axis orientations and displacement patterns of fault surfaces. Journal of Structural Geology 18, 235–248.

Nicol, A., Walsh, J.J., Watterson, J., Underhill, J.R., 1997. Displacement rates of normal faults. Nature 390, 157–159.

Perissoratis, C., Mitropoulos, D., Angelopoulos, I., 1986. Marine geological research at the E. Korinthiakos Gulf. Special Issue of Geology and Geophysical Research. Institute of Geology and Mineral Exploration, Athens, Greece.

Roberts, G.P., 1996a. Variation in fault-slip directions along active and segmented normal fault systems. Journal of Structural Geology 18, 835–845.

Roberts, G.P., 1996b. Noncharacteristic normal faulting surface ruptures from the Gulf of Corinth, Greece. Journal of Geophysical Research 101, 25255–25267.

Roberts, G.P., Gawthorpe, R.L., 1995. Strike variation in deformation and diagenesis along segmented normal faults: an example from the eastern Gulf of Corinth, Greece. In: Lambiase, J.J. (Ed.), Hydrocarbon Habitat in Rift Basins, Geological Society of London Special Publication, 80, pp. 57–74.

Roberts, S., Jackson, J., 1991. Active normal faulting in central Greece: an overview. In: Roberts, A.M., Yielding, G, Freeman, B (Eds.), The Geometry of Normal Faults, Geological Society of London Special Publication, 56, pp. 125–142.

Valensise, G., Ward, S., 1991. Long-term uplift of the Santa-Cruz coastline in response to repeated earthquakes along the San Andreas fault. Bulletin of the Seismological Society of America 81, 1694–1704.

Vita-Finzi, C., 1993. Evaluating late Quaternary uplift in Greece and Cyprus. In: Pritchard, H.M., Alabaster, T., Harris, N.B.W., Neary, C.R. (Eds.), Magmatic Processes and Plate Tectonics, Special Publication of the Geological Society of London, 76, pp. 417–424.

Vita-Finzi, C., King, G.C.P., 1985. The seismicity, geomorphology and structural evolution of the Corinth area of Greece. Philosophical Transactions of the Royal Society of London A314, 379–407.

Walsh, J.J., Watterson, J., 1988. Analysis of the relationship between displacements and dimensions of faults. Journal of Structural Geology 10, 239–247.